Climate Data Record (CDR) Program

Climate Algorithm Theoretical Basis Document (C-ATBD)

Aerosol Optical Thickness

CDR Program Document Number: CDRP-ATBD-0096
Originator Document Number: N/A
Revision 1.0 / March 7, 2011

RESPONSIBILITY

Prepared By:	Xuepeng Zhao	Physical Scientist	NOAA/NCDC
	Signature		Date
Edited By:	Brian Newport	Lead Software Eng.	CDR Program
	Signature		Date
Reviewed By:	<Name>	<Title>	<Organization>
	Signature		Date
Approved By:	<Name>	<Title>	<Organization>
	Signature		Date
Approved By:	<Name>	<Title>	<Organization>
	Signature		Date

REVISION HISTORY

Version	Description	Revised Sections	Date
1.0	Initial submission to CDR Program	New Document	02/24/2011

TABLE of CONTENTS

LIST of FIGURES

LIST of TABLES

ACRONYMS AND ABBREVIATIONS

Acronym or Abbreviation	Meaning
6S	Second Simulation of the Satellite Signal in the Solar Spectrum
ABI	Advanced Baseline Imager
AERONET	AErosol Robotic NETwork
AOT	Aerosol Optical Thickness
APDPS	AVHRR PATMOS-x Data Processing System
AVHRR	Advanced Very High Resolution Radiometer
CATBD	Climate Algorithm Theoretical Basis Document
CDR	Climate Data Record
CM	Cloud Mask
EOS	Earth Observing System
GAC	Global Area Coverage
GACP	Global Aerosol Climate Project
HDF	Hierarchical Data Format
ISCCP	International Satellite Cloud Climatology Project
LLT	Linear Long-term Trend
LUT	Lookup Table
MISR	Multi-angle Imaging SpectroRadiometer
MODIS	Moderate Resolution Imaging Spectroradiometer
NASA	National Aeronautics and Space Administration
NCDC	National Climatic Data Center
NOAA	National Oceanic and Atmospheres Administration
PATMOS	The AVHRR Pathfinder Atmosphere
PATMOS-x	PATMOS Extension
RTM	Radiative Transfer Model
SDS	Scientific Data Sets
SeaWiFS	Sea-viewing Wide Field-of-view Sensor
STD	Standard Deviation
SWIR	Shortwave Infrared
TOA	Top of Atmosphere
VIIRS	Visible/Infrared Imager Radiometer Suite

1. Introduction

1.1 Purpose

The purpose of this document is to describe in detail the algorithm submitted to the National Climatic Data Center (NCDC) by Xuepeng (Tom) Zhao/NCDC that will be used to create the Aerosol Optical Thickness Climate Data Record (CDR), using the AVHRR PATMOS-x Data Processing System (APDPS). The actual algorithm is defined by the computer program (code) that accompanies this document, and thus the intent here is to provide a comprehensive guide to understanding that algorithm.

1.2 Definitions

Following is a summary of the symbols used to define the algorithm.

Spectral and directional parameters:

$$\lambda = \textit{wavelength of retrieval channels.} \quad (1)$$

$$\theta_s = \textit{solar zenith angle.} \quad (2)$$

$$\theta_v = \textit{view zenith angle.} \quad (3)$$

$$\phi_{sv} = \textit{relative azimuth angle.} \quad (4)$$

$$\eta = \textit{glint angle.} \quad (5)$$

Atmospheric parameters:

$$\tau = \textit{aerosol optical thickness.} \quad (6)$$

$$\rho = \textit{reflectance or radiance .} \quad (7)$$

2. Observing Systems Overview

2.1 Products Generated

The objective of this algorithm is to retrieve the aerosol optical thickness (AOT) from NOAA operational AVHRR sensor (such as NOAA-14) pixels at selected spatial (such as 8-km) and temporal (such as 1 time per day) resolution in cloud free condition during daytime. The final product is mapped into 0.5^ox0.5^o equal area grid (total 165018 grids over the globe). Due to the relatively large uncertainties associated with surface reflectance over water glint area and land surface as well as limited AVHRR retrieval channels, the current algorithm only performs retrieval over non-glint water surface (specifically at the anti-solar side of the orbit and viewing angle is larger than 40^o away from the specular ray). The primary retrieval product is AOT at 0.63μm. However AOT

at 0.83μm (or 1.61μm) is also retrieved for consistent check purpose. The standard deviation (STD) of AOT at 0.63μm is also calculated for each 0.5^{o}x0.5^{o}equal area grid.

2.2 Instrument Characteristics

The aerosol products will be generated for each cloud-free pixel (8km x 8km) observed by the AVHRR imager. The aerosol retrieval makes use of 2 channels to 3 channels from visible to near-infrared bands depending on a specific AVHRR sensor and its available channels (Table1 is an example for AVHRR instrument) where aerosol signal is relatively strong but gas absorption is weak. The channels used for detecting unfavorable retrieval conditions (such as over land) are still under investigation; therefore, the channels used in current algorithm are subject to change as development continues.

Channel number	Wavelength (μm)	Aerosol retrieval over water
1	0.63	X (AOT)
2	0.83	X (AOT)
3a	1.61	X (AOT)
3b	3.75	
4	11.0	
5	12.0	

Table 1: Example of AVHRR channels and the channels selected for aerosol retrieval. Channel 3a is only available for the AVHRR instrument on NOAA-15, -16, -17, -18, -19.

3. Algorithm Description

3.1 Algorithm Overview

This is the complete description of the algorithm at the current level of maturity (which will be updated with each revision). The algorithm is developed for aerosol retrieval over ocean only since SWIR channel (e.g., 2.13μm) required generally for the aerosol retrieval over land is not available from AVHRR instrument. The aerosol retrieval module is embedded in the AVHRR PATMOS-x Data Processing System (http://cimss.ssec.wisc.edu/patmosx/). The retrieval system includes two units: daily AOT product unit and monthly AOT product unit. The aerosol retrieval algorithm provides estimates of aerosol optical thickness (AOT or τ) in the visible (0.63μm) and near infrared (0.83μm or 1.61μm) channels of AVHRR instrument (Zhao et al., 2004, 2008), assuming the molecular atmosphere, aerosol microphysics, and surface reflectance are known. In practice, the relationship between aerosol optical thickness, τ, and dimensionless top-of-atmosphere (TOA) apparent reflectance, ρ, (radiance normalized to solar flux at the top of the atmosphere) is described by a 4-dimensional lookup table (LUT), pre-calculated for different τ, solar and viewing geometries using the 6S radiative transfer model (Vermote et al., 1997a,b). The clear-sky reflectances of

AVHRR in channel 1 (0.63μm) and 2 (0.83μm) or 3a (1.61μm) are input to the retrieval scheme. Aerosol optical thickness (τ_1 and τ_2) are retrieved independently from both channels. For this reason the algorithm is described as an “independent” two-channel algorithm. A weak absorbing aerosol model and a bimodal log-normal size distribution are used in the 6S code for the generation of LUTs. Other parameters specified as input to the LUTs are Lambertian oceanic reflectance with diffuse glint correction to the aerosol phase function. Detailed explanation of this aerosol retrieval algorithm is presented in the following sections.

3.2 Processing Outline

The processing outline of the AVHRR PATMOS-x Data Processing System (APDPS) and the embedded AOT retrieval module are summarized in the Figures 1 and 2, respectively, which includes the basic sections as input, output, and aerosol retrievals over water. The algorithm to create aerosol product is written in FORTRAN-90. Input data is AVHRR level-1B in binary format and output products are written in HDF format.

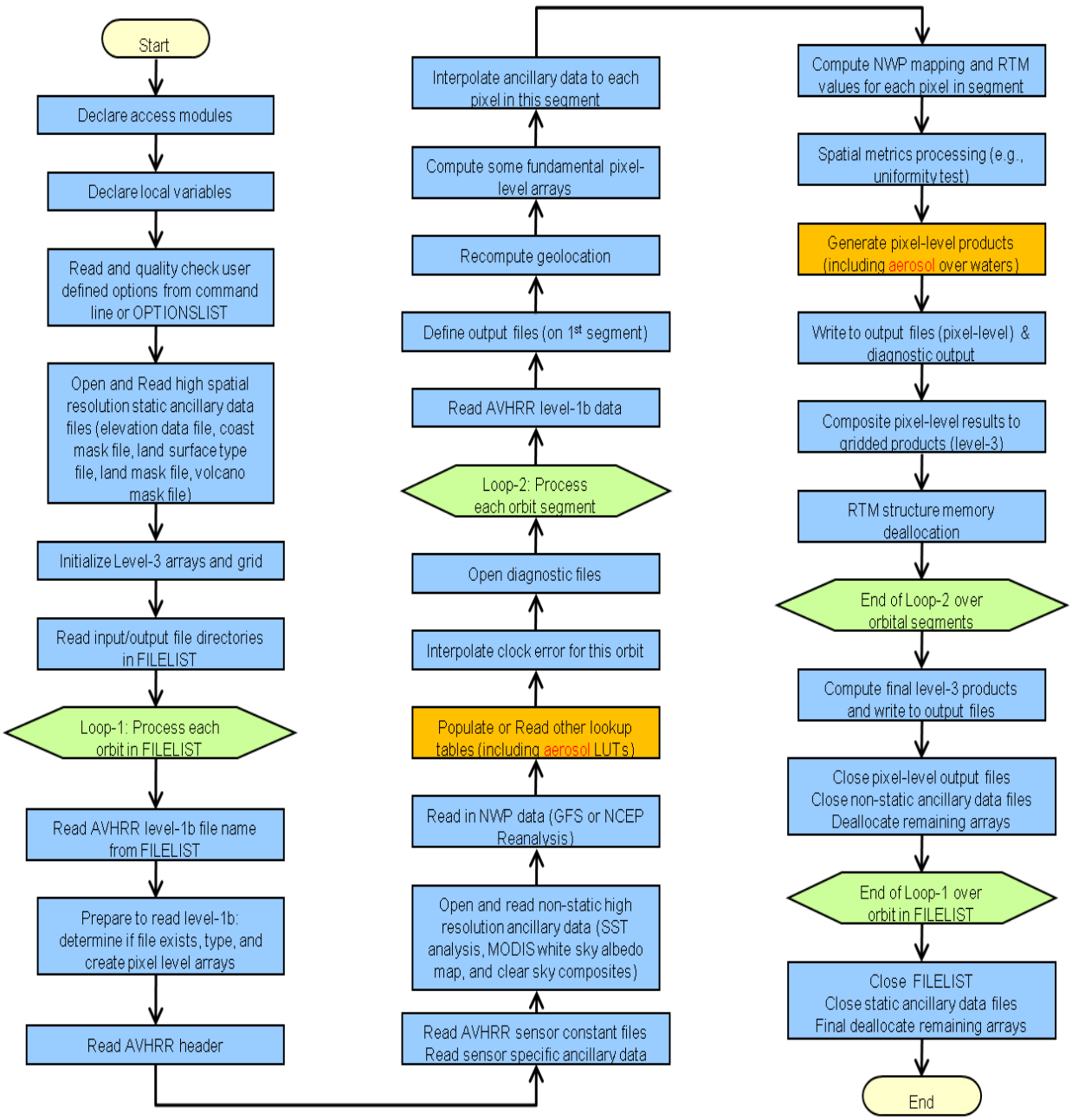

Figure 1: High level flowchart of the AVHRR PATMOS-x Data Processing System (APDPS), illustrating the main processing sections (aerosol sections are highlighted with bright color).

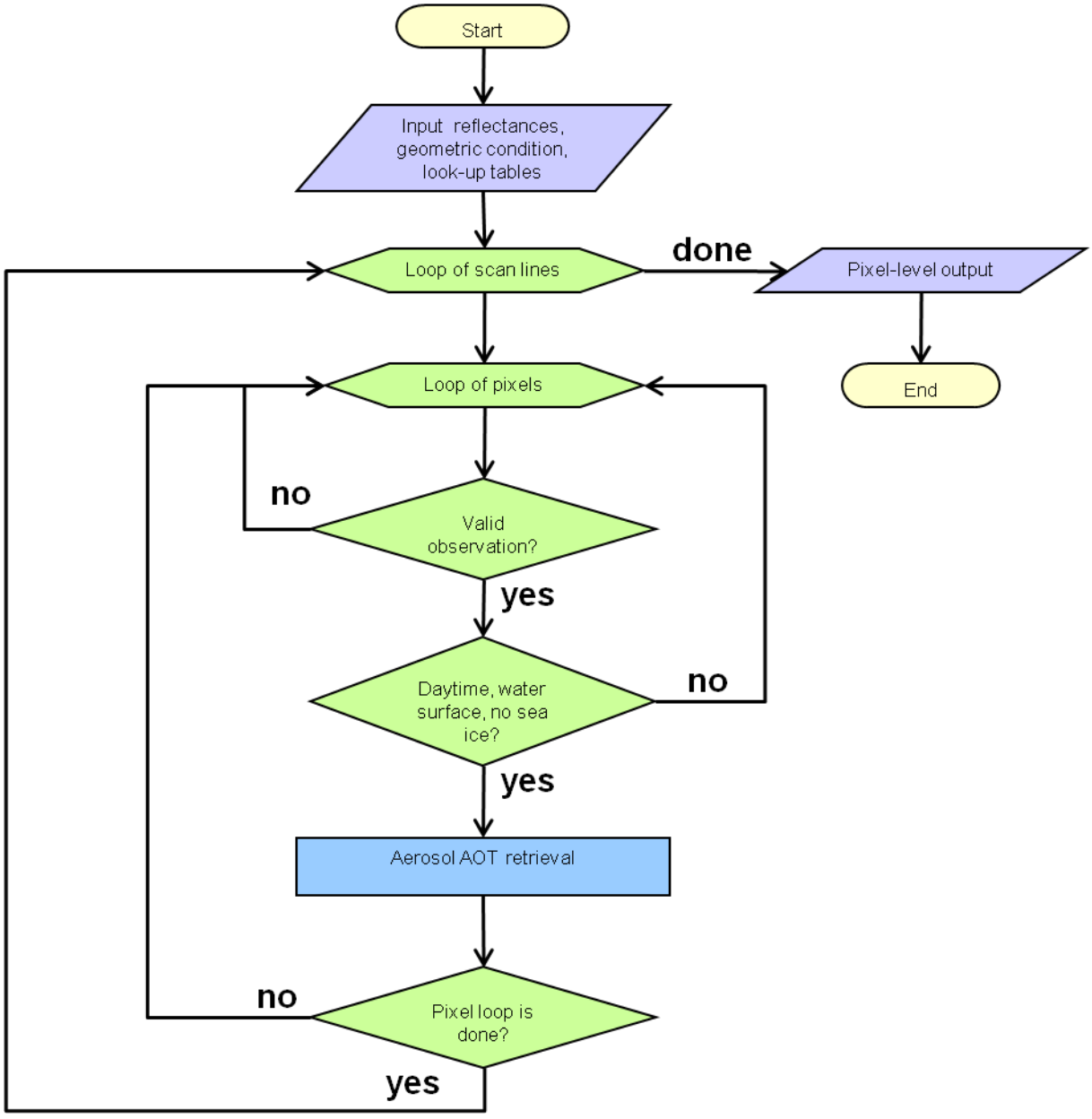

Figure 2: High level flowchart of the AOT retrieval in the APDPS, illustrating the main processing sections.

3.3 Algorithm Input

3.3.1 Primary Sensor Data

Table 2 lists the primary sensor data used by the aerosol retrieval, including calibrated and geolocated AVHRR Global Area Coverage (GAC) 'Level 1B' reflectance at 3 channels from AVHRR sensor, geolocation information, and sensor data quality flags. Here we also include channel 3a even though this channel is only available for the AVHRR sensors onboard NOAA-15 and follow-on satellites.

Name	Type	Description	Dimension (spatial resolution)
Ch1 reflectance	Input	Calibrated channel 1 reflectance at 0.63μm	Scan line (4km x 4km)
Ch2 reflectance	Input	Calibrated channel 2 reflectance at 0.83μm	Scan line (4km x 4km)
Ch3a reflectance	Input	Calibrated channel 3a reflectance at 1.61μm	Scan line (4km x 4km)
Latitude	Input	Pixel latitude	Scan line (4km x 4km)
Longitude	Input	Pixel longitude	Scan line (4km x 4km)
Solar geometry	Input	Solar zenith and azimuth angles	Scan line (4km x 4km)
View geometry	Input	View zenith and azimuth angles	Scan line (4km x 4km)
QC flags	Input	Quality control flags with level 1B data	Scan line (4km x 4km)

Table 2: Primary AVHRR sensor GAC input data for aerosol retrieval.

3.3.2 Ancillary Data

The aerosol algorithm requires two ancillary input datasets: 1) Cloud mask (CM) input (Table 3) from cloud retrieval system in the AVHRR PATMOS-x Data Processing System; 2) Static look-up tables (LUTs) for atmosphere (molecular + aerosol + surface)(Table 4).

Name	Type	Description	Dimension (spatial resolution)
Cloud info.	Input	Internally from APDPY level 2 CM data	Scan line (8km x 8km)
Land/water info.	Input	Internally from APDPY level 2 CM data	Scan line (8km x 8km)
Sunglint info.	Input	Internally from APDPY level 2 CM data	Scan line (8km x 8km)
Snow/ice info.	Input	Internally from APDPY level 2 CM data	Scan line (8km x 8km)

Table 3: PATMOS-x cloud mask (CM) input data.

Name	Type	Description	Dimension
Ch1 LUT	Input	TOA apparent reflectance at 0.63μm channel as function of solar zenith angle, relative azimuth angle, view zenith angle, and aerosol optical thickness	15 x 19 x 15 x 7
Ch2 LUT	Input	TOA apparent reflectance at 0.83μm channel as function of solar zenith angle, relative azimuth angle, view zenith angle, and aerosol optical thickness	15 x 19 x 15 x 7
Ch3a LUT	Input	TOA apparent reflectance at 1.61μm channel as function of view zenith angle, relative azimuth angle, solar zenith angle, and aerosol optical thickness	15 x 19 x 15 x 7

Table 4: Look-up table (LUT) input data.

3.3.3 Derived Data

Not Applicable.

3.3.4 Forward Models

Not applicable.

3.4 Theoretical Description

The feasibility of aerosol retrieval from satellite-observed radiances is based on the fact that these radiances are affected by the physical and chemical properties of aerosols (Ackerman, 1997). The AVHRR algorithm retrieves the aerosol optical thickness from reflectance (or radiances) observed in the AVHRR visible and near infrared channels. The assumption is that the contributions of the molecular atmosphere and ocean surface can be accurately computed, and the aerosol can be represented by an averaged oceanic aerosol model based on AERONET observations (see Holben et al., 1998, 2001).

3.4.1 Physical and Mathematical Description

3.4.1.1 Strategy

The ocean/water AOT retrieval algorithm is based on a look-up table approach. A set of top-of-atmosphere (TOA) apparent reflectance (including contributions from molecular, aerosol, and surface) are pre-computed for each AVHRR retrieval channel by using a radiative transfer model, such as 6S model (Vermote et. al., 1997b), and stored in LUTS. For each retrieval channel, TOA reflectance from the LUT is compared with the observed reflectance through interpolation for a given solar-view geometry and a set of aerosol optical thickness to find the best match. The corresponding AOT for the best

match is the retrieval solution. The AOT retrieval algorithm has been illustrated schematically in the above Figure 2.

3.4.1.2 Aerosol Model

Aerosol model is represented by the combination of a fine lognormal and a coarse lognormal mode given in Eq. (8).

$$\frac{dN(r)}{d\ln r} = \sum_{i=1}^{2} \frac{N_0}{\sqrt{2\pi}\ln\sigma_{g,i}} \exp\left[-\frac{\left(\ln r - \ln r_{g,i}\right)^2}{2\left(\ln\sigma_{g,i}\right)^2}\right] \qquad (8)$$

where $N(r)$ is the number density corresponding to particles of radius within (r, r+dr), $r_{g,i}$ is the geometric mean radius, and $\sigma_{g,i}$ is the associated standard deviation of the radius. The fine and coarse modes are adopted from AERONET observation and summarized in Table 5 along with their microphysical properties. These microphysical properties were determined from the validation of the AVHRR aerosol retrievals against the AERONET observations (see Zhao et al., 2002, 2004).

Aerosol Model	r_g	σ_g	**Refractive index at retrieval wavelength (μm)**		
			0.63	0.83	1.61
Fine Mode	0.044	1.96	1.45 - 0.005i	1.45 – 0.007i	1.45 – 0.005i
Coarse Mode	0.370	2.370	1.45 - 0.005i	1.45 – 0.007i	1.45 – 0.005i

Table 5: Microphysical properties of ocean aerosol model used in the AOT algorithm, including geometric mean radius (r_g), standard deviation (σ_g), and refractive index.

3.4.1.3 Modeling TOA reflectance over ocean

Following the 6S radiative transfer model (RTM) (Vermote, 1997a), the spectral reflectance at the satellite level (ρ_{toa}) is a combination of radiation from the surface (ρ_{surf}) and the atmosphere (ρ_{atm}) due to reflection, scattering by molecules and aerosols and absorption by aerosols and gases as shown in Eq. (9):

$$\rho_{toa} = \rho_{atm} + \rho_{surf} \qquad (9)$$

Here the spectral (or channel) index is omitted for simplicity. To facilitate the calculation of atmospheric reflection with varying gaseous amount and surface pressure, gas absorption, aerosol and Rayleigh scattering are decoupled by assuming a three-layer vertical model, where ozone and other minor absorbing gases (O_2, CO_2, N_2O, CH_4) (except water vapor) is on the top layer, molecular scattering in the middle layer, and the well-mixed aerosol and water vapor at the bottom layer. Without the consideration of interaction between aerosol and Rayleigh scattering, the atmospheric contribution to TOA reflectance is computed as:

$$\rho_{atm} = T^{O_3} T^{og} \left[(\rho_{R+A} - \rho_R(P_0)) T^{\frac{1}{2}H_2O} + \rho_R(P) \right] \quad (10)$$

where,

T^{O_3} is ozone transmittance,

T^{og} is the gas transmittance other than ozone and water vapor,

T^{H_2O} is the total column water vapor transmittance,

$T^{\frac{1}{2}H_2O}$ is the half column water vapor transmittance,

ρ_{R+A} is the path reflectance by aerosols and molecules at standard pressure,

$\rho_R(P_0)$ is the Rayleigh reflectance from molecules at standard pressure = 1atm,

$\rho_R(P)$ is the Rayleigh reflectance from molecules at the actual pressure .

By given the profiles of atmosphere (e.g., middle-latitude summer), greenhouse gases, aerosols (including aerosol model), these terms and the atmospheric reflectance (ρ_{atm}) are calculated directly from 6S code.

The reflectance of ocean surface is modeled as Lambertian dark water surface with diffuse glint correction according to Breon (1993). The Lambertian surface reflectance is calculated directly from 6S code. The surface albedos used are 0.02, 0.01, and 0.002 respectively for 0.63, 0.83, and 1.61μm retrieval channels. The diffuse glint correction is calculated separately following Eq (21) in Breon (1993) and applied to the 6S modeling to obtain ρ_{surf}. Combined ρ_{atm} and ρ_{surf} are used to determine ρ_{toa} from Eq. (9) and stored in LUTs for retrieving use.

3.4.2 Calculations

The retrieval is performed for 1) solar zenith angle $\theta_s < 70^o$ and view zenith angle $\theta_v < 60^o$ to minimize atmospheric curvature effects; 2) glint angle $\eta > 40^o$ to avoid sun glint contamination; 3) relative azimuth angle $\phi_{sv} > 90^o$ (the anti-solar side of satellite orbit) to include only back scattering. For a given pixel (observing geometry), the model TOA apparent reflectance in LUTs for a retrieval channel is compared with observations to determine the optimal solution through interpolation. The AOT value corresponding to the best match of apparent reflectance is the final retrieved AOT for this pixel. The retrieval is performed according to two layer loops: outer layer is scanline loop and inner layer is pixel loop. For the pixels do not meet the retrieval conditions, a fill value is provided. The pixel level AOT retrievals are averaged to generate product in 0.5^ox0.5^o equal area grid, which is written to output. As needed, this gridded daily AOT product

can be further averaged to produce monthly AOT product on the same grids. This monthly averaging is a function of AVHRR PATMOS-x Data Processing System.

3.4.3 Look-Up Table Description

As the backbone of AVHRR AOT retrieval, LUTs for three retrieval channels are generated with the non-vector version of 6S radiative transfer code. The TOA apparent reflectance for a set of solar-view geometries (view zenith angle, relative azimuth angle, and solar zenith angle) and aerosol optical thickness are pre-calculated for the selected aerosol mode given in Section 3.4.1.2 for three retrieval channels and are stored in three 4-dimension tables, respectively. Reflectance contribution of molecular, aerosol, and surface are all included in the stored reflectance. The middle latitude summer atmosphere and Lambertian dark water surface with diffuse glint correction on aerosol phase function are used for generating LUT. The surface albedos are set to 0.02, 0.01, and 0.002 in the 6S input cards for AVHRR 0.63, 0.83, and 1.61μm channels, respectively, for the generation of LUTs. The arguments and dimensions of the LUTs are given in Table 6. The corresponding 7 AOT bin values at 0.55μm (needed for 6S input card) for the aerosol model used are 0.000, 0.164, 0.328, 0.656, 0.984, 1.311, and 1.638.

Argument		Dimension	Bins
View zenith angle (^{o})		15	0.0, 6.0, 12.0, 18.0, 24.0, 30.0, 36.0, 42.0, 48.0, 54.0, 60.0, 66.0, 72.0, 78.0, 84.0
Relative azimuth angle (^{o})		19	0.0, 10.0, 20.0, 30.0, 40.0, 50.0, 60.0, 70.0, 80.0, 90.0, 100.0, 110.0, 120.0, 130.0, 140.0, 150.0, 160.0, 170.0, 180.0
Solar zenith angle (^{o})		15	0.0, 6.0, 12.0, 18.0, 24.0, 30.0, 36.0, 42.0, 48.0, 54.0, 60.0, 66.0, 72.0, 78.0, 84.0
AOT	at 0.63μm channel	7	0.000, 0.147, 0.294, 0.588, 0.882, 1.176, 1.470
	at 0.83μm channel	7	0.000, 0.113, 0.226, 0.452, 0.678, 0.904, 1.130
	at 1.61μm channel	7	0.000, 0.082, 0.164, 0.328, 0.492, 0.656, 0.820

Table 6: Arguments and dimensions of three LUTs.

3.4.4 Algorithm Output

The pixel level retrievals are mapped to 0.5^ox0.5^o equal area grid (total 165018 grids over the globe) and write to output using the output functions of AVHRR PATMOS-x Data Processing System. There are two output products. The first is daily gridded product which is the result from averaging pixel level (8km x 8km) retrievals. The second is monthly gridded product, which is the result from averaging daily product. Both products are in HDF format. The AOT values are stored as a 1-D Scientific Data Sets (SDS) array. The size of one daily output file is between 1.5 to 9MB and one

monthly output file is between 26-30MB. The summary of the two output products are provided in Table 7 and 8, respectively.

Name	Type	Description	Spatial Resolution
cell_index	output	Index of cell: 1-165018	0.5^o x 0.5^o
cell_longitude	output	Longitude of cell center	0.5^o x 0.5^o
cell-latitude	output	Latitude of cell center	0.5^o x 0.5^o
spacecraft_id	output	ID of this craft; e.g., 14 means NOAA-14	0.5^o x 0.5^o
asc_des_flag	output	Ascending /descending flag; 0=ascending	0.5^o x 0.5^o
orbit_number	output	Number of this orbit	0.5^o x 0.5^o
utc_time	output	UTC time in hours	0.5^o x 0.5^o
jday	output	Julian day	0.5^o x 0.5^o
year	output	4 digit year	0.5^o x 0.5^o
sensor_zenith	output	Sensor zenith angle; degree	0.5^o x 0.5^o
solar_zenith	output	Solar zenith angle; degree	0.5^o x 0.5^o
relative_azimuth	output	Relative azimuth angle; degree	0.5^o x 0.5^o
glint_zenith	output	Glint zenith angle; 0=center of specular reflection	0.5^o x 0.5^o
aot1	output	Mean channel 1 AOT	0.5^o x 0.5^o
aot1_std	output	STD of aot1	0.5^o x 0.5^o
aot2*	output	Mean channel 2 (or 3a) AOT (* this is an optional output)	0.5^o x 0.5^o

Table 7: Daily aerosol CDR output data.

Name	Type	Description	Spatial Resolution
cell_index	output	Index of cell: 1-165018	0.5^o x 0.5^o
cell_longitude	output	Longitude of cell center	0.5^o x 0.5^o
cell-latitude	output	Latitude of cell center	0.5^o x 0.5^o
spacecraft_id	output	ID of this craft; e.g., 14 means NOAA-14	0.5^o x 0.5^o
utc_time_mean	output	Averaged UTC time in hours	0.5^o x 0.5^o
year	output	4 digit year	0.5^o x 0.5^o
sensor_zenith_mean	output	Averaged sensor zenith angle; degree	0.5^o x 0.5^o
solar_zenith_mean	output	Averaged solar zenith angle; degree	0.5^o x 0.5^o
relative_azimuth_mean	output	Averaged relative azimuth angle; degree	0.5^o x 0.5^o
aot1_mean	output	averaged channel 1 AOT	0.5^o x 0.5^o
aot1_max	output	Maximum value of channel 1 AOT	0.5^o x 0.5^o
aot1_min	output	Minimum value of channel 1 AOT	0.5^o x 0.5^o
aot1_count	output	Number of daily channel 1 AOT used for monthly mean calculation	0.5^o x 0.5^o

Table 8: Monthly aerosol CDR output data.

4. Test Datasets and Outputs

4.1 Test Input Datasets

The algorithm is used to produce aerosol CDR from long-term operational AVHRR observations. Thus, long-term AVHRR level-1B Global Area Coverage (GAC) data (in a spatial resolution of 4km x 4km) from 1981 to 2009 are used as input data. Current version (version 1) of the aerosol retrieval algorithm is incorporated directly in the AVHRR PATMOS-x Data Processing System (APDPS) as a module so that the aerosol retrieval is a part of the APDPS. Specifically, the AVHRR level-1B data are read by the APDPS and the radiances (or reflectances) used for the retrieval are re-calibrated in the APDPS by using the new calibration coefficients. The new calibration coefficients are obtained offline by comparing the match-ups between accurate MODIS radiance and AVHRR radiances (Heidinger et al., 2002, 2010; Molling et al., 2010). The cloud mask scheme in the APDPS is used to find the clear-sky radiances (or reflectances) in 2x2 pixels (Pavolonis et al., 2004, 2005). The clear-sky radiances (in a spatial resolution of 8km x 8km) identified by CM scheme is used by aerosol retrieval module in the APDPS to complete aerosol retrievals in 8km x8km spatial resolution, which are further averaged to 0.5^o x 0.5^o equal area and write to APDPS output in a daily step. Please refer to the website (*http://www.ncdc.noaa.gov/cdr/operationalcdrs.html*) of the NCDC CDR program for more information on the APDPS.

4.2 Test Output Analysis

4.2.1 Examples of Products

An example of daily AOT product (at 0.63μm channel) for January 1, 2005 is plotted in Figure 3. 16 AOT swaths correspond to 16 satellite orbits in a day. This daily data are further averaged to form monthly product as shown in Figure 4 for January 2005.

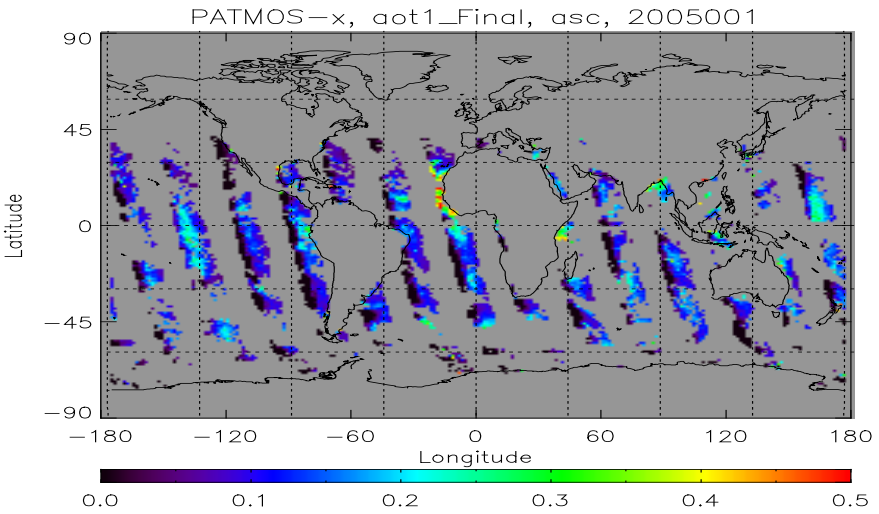

Figure 3: Example of AOT (at 0.63μm channel) daily (January 1, 2005) product.

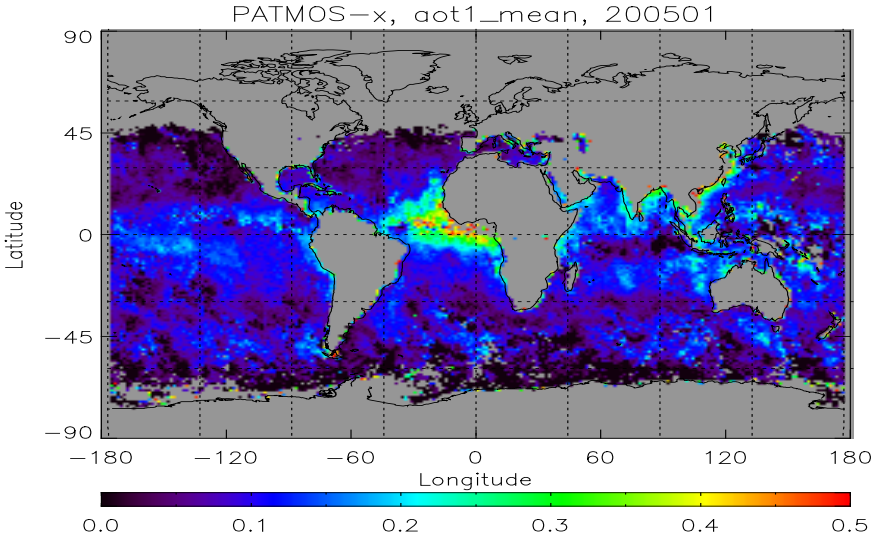

Figure 4: Example of AOT (at 0.63μm channel) monthly (January, 2005) product.

Example of AOT time series for our monthly product is shown as the black curve in Figure 5. At the same time, we also overlay the AOT time series from GACP aerosol

data (ISCCP/AVHRR based aerosol product), EOS/MISR, and EOS/MODIS aerosol data. We can see these time series agree reasonably well with each other.

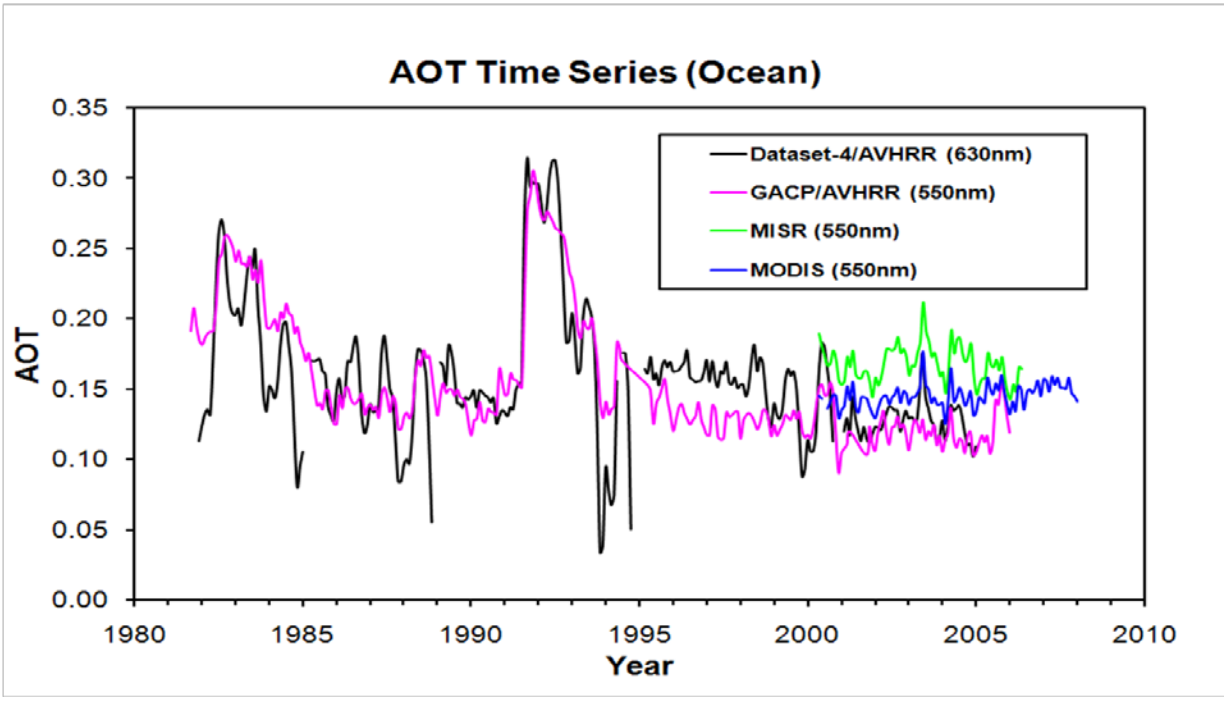

Figure 5: Examples of AOT time series from AVHRR, GACP, MISR, and MODIS.

4.2.2 Validations

The validation and evaluation is a continuous effort in the development of the retrieval algorithm so that it will be updated from time to time. Both comparison with ground truth (such as AERONET observations) and inter-satellite comparison are performed to validate and evaluate the performance of our retrieval algorithm, which are presented below. The objective is to determine the precision and accuracy of the aerosol retrievals.

4.2.2.1 Comparisons with the Surface AERONET Observations

AERONET observations (see Holben et al., 1998, 2001) are commonly used as ground truth for the validation of satellite aerosol retrievals (e.g., Hsu et al., 1999; Chu et al., 2002; Remer et al., 2002; Torres et al., 2002; Zhao et al., 2002, 2004; Kahn et al., 2005). We have selected 9 AEONET island stations which cover the major regimes of global oceanic aerosol characteristics as our validation sites. Three years (1998-2000) of quality assured level 2 AERONET aerosol optical thickness observations (temporally averaged within ±1-hour window around AVHRR overpass) are used as our ground truth and collocated with AVHRR aerosol retrievals (spatially averaged in a 100x100 km box). Total 599 match-up points have been found and used for validation statistics. Detailed validation approach and results can be found in Zhao et al. (2002, 2004). The

validation results for the retrievals at 0.63 and 0.83μm are shown in Figure 6. The systemic and random errors of the global AOT retrievals are summarized in Table 9.

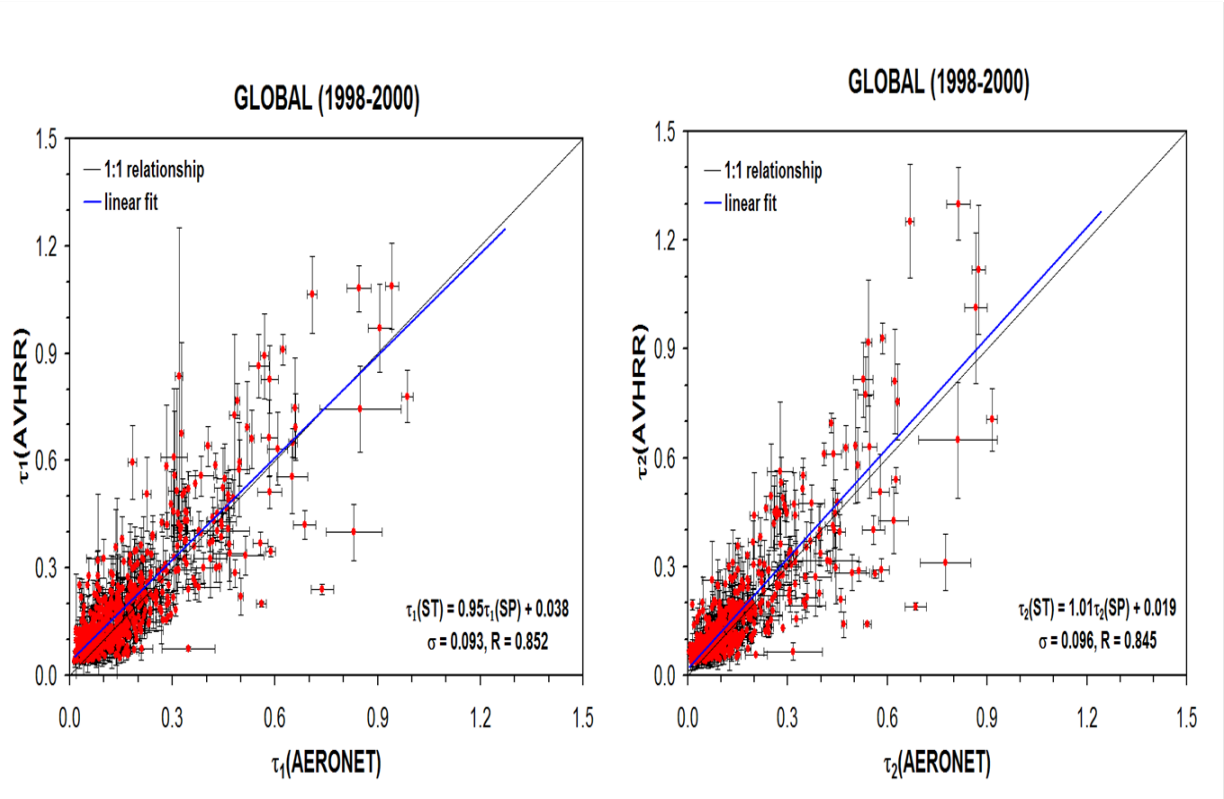

Figure 6: Scatter plots of AVHRR retrievals versus AERONET observations for 0.63μm channel (left panel) and 0.83μm channel (right panel).

AVHRR Channel	Systematic Errors			Random Error (±)
	Minimum (τ = 0.00)	Mean (τ = 0.15 at λ_1) (τ = 0.11 at λ_2)	Maximum (τ = 1.00)	
λ_1=0.63μm	0.031	0.030	0.024	0.113
λ_2=0.83μm	0.032	0.032	0.035	0.103

Table 9: Systematic and random errors for the AVHRR AOT retrieval based on surface AERONET validation.

4.2.2.2 Comparison with other Satellite Aerosol Retrievals

MODIS instrument on the NASA EOS satellite is one of the most comprehensive radiometric imager and has the channels similar to almost all the past, current, and future operational and research radiometric imagers (e.g., AVHRR, SeaWiFS, VIIRS,

ABI, etc.). Thus, MODIS observations can be used as proxy data for examining the performance of our aerosol retrieval algorithm running for different radiometric imagers. For example, we can pick up the MODIS observations in the channels similar to AVHRR instruments and make retrieval using our independent two-channel algorithm (called AVHRR-type retrieval). Thus, comparison between AVHRR-type retrieval and the MODIS retrieval is an effective method for evaluating the performance of our independent 2-channel aerosol retrieval algorithm. One example is given in Figure 7, which compares MODIS AOT retrieval at 0.66μm with our AVHRR-type AOT retrieval in April 2001. The left plot shows the difference map (AVHRR-MODIS) and the right plot shows the corresponding scatter plot. Our AVHRR-type AOT retrieval compares reasonably well with the MODIS retrieval when AOT values are lower (e.g., over remote ocean surface) but is somewhat higher than the MODIS retrieval when AOT values are higher (e.g., over coast ocean surface). For a global average, the two AOTs compares reasonably well considering $\Delta\tau_1$ (AVHRR-MODIS) = -0.009. More inter-comparison studies can be found in Zhao et al. (2005a, b).

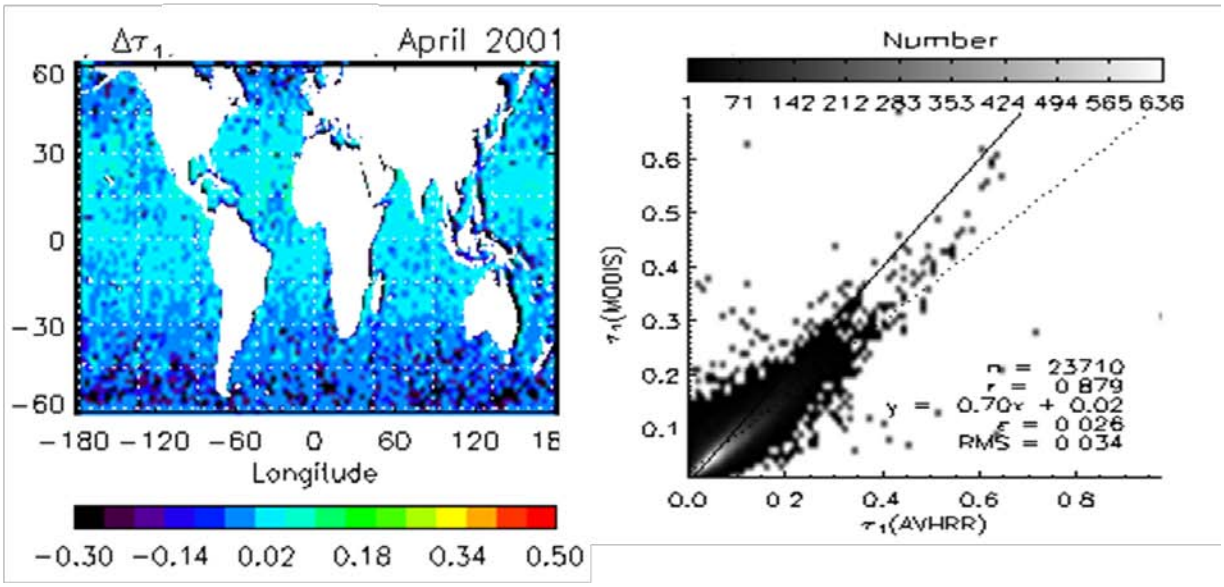

Figure 7: Difference between MODIS AOT retrieval and AVHRR-type AOT retrieval.

4.2.2.3 Comparison of AOT Time Series and Long-term Trends

Since the aerosol optical thickness (AOT) product from our aerosol retrieval algorithm is used as climate data record (CDR) so that we also check the time series and long-term trend derived from our AOT product. The above Figure 5 shows the comparison of our AOT time series with that from GACP, MISR, and MODIS aerosol data. We can see these time series agree reasonably well with each other. Figure 8 further displays the linear long-term trend (LLT) and its significance for our seasonal mean AOT at 0.63μm averaged over the globe. Decreasing tendency with high confidence is detected in spring (MAM) and summer (JJA). We also compare the linear long-term trend (LLT)

from our AOT data with the LLT derived from other satellite long-term AOT data, such as global aerosol climate project (GACP) data (Mishchenko and Geogdzhayev, 2007, Mishchenko et al., 2007) derived from ISCCP/AVHRR dataset. One example of the comparison with the GACP AOT LLT is shown in Figure 9. Both datasets are based on the AVHRR observations but with independent calibration, cloud screening, and aerosol retrieval algorithm. Both datasets show a decreasing LLT for the southern hemisphere (SH), northern hemisphere (NH), and globe and the decreasing trend in the NH is more evident than in the SH. Almost all detected tendencies from the two datasets are above 95% confidence level except in the SH of our data. More detailed studies on aerosol long-term trends using our retrieved data can be found in Li et al. (2009) and Zhao et al. (2008, 2011).

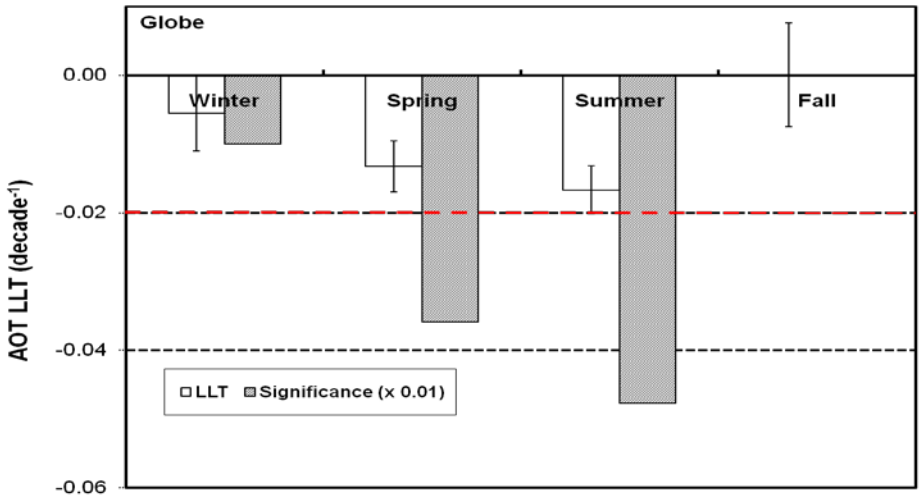

Figure 8: Column plot of the LLT and its significance for seasonally averaged AOT at 0.63μm from our aerosol CDR data. The vertical bar line is ±standard deviation. The significance is scaled by 0.01 for display and the red dash line is 95% confidence line.

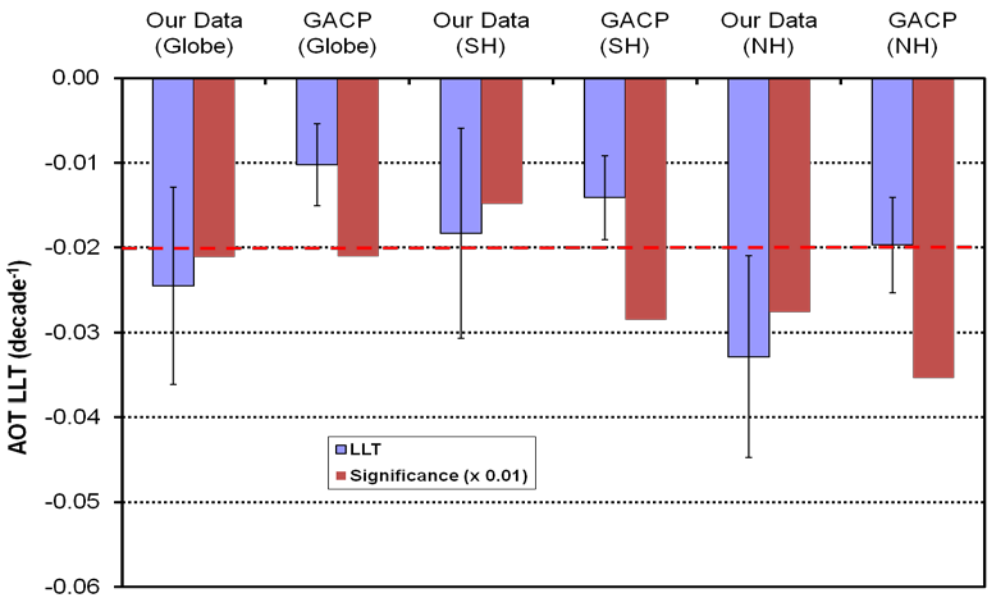

Figure 9: Column plot of the LLT and its significance for annual mean AOT at 0.63μm from our aerosol data and at 0.55μm from the GACP data. The vertical bar line is ±standard deviation. The significance is scaled by 0.01 for display and the red dash line is 95% confidence line. Values over the globe, the southern hemisphere (SH), and the northern hemisphere (NH) are displayed together.

5. Practical Considerations

5.1 Numerical Computation Considerations

a. LUT is used for increasing speed.

b. Linear interpolation of LUT values.

5.2 Programming and Procedural Considerations

a. Pixel by pixel retrieval but aggregated into 0.5^{o}x0.5^{o} for output.

c. Calibrated and geo-located reflectances, cloud mask and snow/ice mask must be available before aerosol retrieval.

d. Program modules are used to ease modification and upgrades.

e. The jobs are run on numerous computers via SSH/troll to speed up the execution and data production in a research oriented computing environment. The batch file is broke up into smaller batch files which are then launched on numerous nodes.

5.3 Quality Assessment and Diagnostics

The following flags or variables will be produced:

- Missing/No data.
- STD of daily AOT for each grid.
- STD, Minimum, and Maximum of monthly AOT for each grid.
- Count of samples for monthly averaging.

5.4 Exception Handling

The quality control flags for aerosol retrieval will be checked and inherited from the flagged Level 1b sensor input data, including bad sensor input data, missing sensor input data and validity of each aerosol channel; and will be checked and inherited from the PATMOS-x cloud mask at each pixel for clear, possibly clear, cloud and possibly cloudy.

The algorithm does checks for conditions not favorable for aerosol retrieval, such as snow/ice pixel, glint area, and viewing geometry.

6. Assumptions and Limitations

This section describes the limitations and assumptions in the current version of the aerosol retrieval algorithm.

6.1 Assumptions

The following assumptions have been made in the current algorithm development:

- Aerosol has globally fixed optical properties;
- Aerosol is in spherical shape and in bi-mode lognormal distribution;
- It is vertically well-mixed;
- Surface is dark and Lambertian with a diffuse glint correction;
- Calibrated and geo-located radiances in AVHRR channels 1-5 are available;
- PATMOS-x cloud mask is available;
- Atmospheric state is fixed.

6.2 Limitations

The limitations of our aerosol retrieval are summarized as below:

f. Perform retrieval only in daytime.

g. Needs accurate clear-sky reflectance.

h. Perform retrieval only over dark ocean surface.

i. Does not account for bidirectional reflectance over ocean.

7. Future Enhancements

The following listed items are our planned improvement on our retrieval and data processing.

a. Run the aerosol retrieval independent from the PATMOS-x data processing system. For example, using CDR clear-sky radiances from level-2 product of the PATMOS-x data processing system as the input for our retrieval.

b. Extend the retrieval to dark land surfaces.

c. Account for bidirectional reflectance over ocean.

d. Continue the validation of the retrieval for more years.

8. References

Ackerman, S. A. (1997). Remote sensing aerosols using satellite infrared observations. *J. Geophys. Res*. 102, 17069–17079.

Breon, F. M. (1993). An analytical model for the cloud free atmosphere/ocean system reflectance. *Remote Sens. Environ.*, 43, 179-192.

Chu, D. A., Y. J. Kaufman, C. Ichoku, L. A. Remer, D. Tanre, B. N. Holben (2002). Validation of MODIS aerosol retrieval over land. *Geophys. Res. Lett.*, 29, doi:10.1029/2001GL013205.

Heidinger, A.K., Cao, C. and Sullivan, J.T. (2002). Using moderate resolution imaging spectrometer (MODIS) to calibrate advanced very high resolution radiometer reflectance channels. *Journal of Geophys. Res.*, 107, 4702, doi:10.1029/2001JD002035.

Heidinger, A.K., Straka III, W.C., Molling, C.C., Sullivan, J.T. and Wu, X. (2010). Deriving an inter-sensor consistent calibration for the AVHRR solar reflectance data record. *International Journal of Remote Sensing*, in press.

Holben B.N., et al. (1998). AERONET - A federated instrument network and data archive for aerosol characterization. *Rem. Sens. Environ.*, 66, 1-16, 1998.

Holben, B.N., et al. (2001). An emerging ground-based aerosol climatology: Aerosol Optical Depth from AERONET. *J. Geophys. Res.*, 106, 12,067-12,097.

Hsu, N. C., J. R. Herman, O. Torres, B. N. Holben, D. Tanre, T. F. Eck, A. Smirnov, B. Chatenet, and F. Lavenu (1999). Comparisons of the TOMS aerosol index with Sun-photometer aerosol optical thickness: Results and applications, *J. Geophys. Res.*, 104, 6269-6279.

Kahn, R., B. Gaitley, J. Martonchik, D. J. Diner, C. A. Crean, and B. Holben (2005). Multiangle Imaging Spectroradiometer (MISR) global aerosol optical depth validation based on 2 years of coincident Aerosol Robotic Network (AERONET) observation. *J. Geophys. Res.*, 110, doi:10.1029/2004JD004706.

Li, Z., T. X.-P. Zhao, R. Kahn, M. Mishchenko, L. Remer, K.-H. Lee, M. Wang, I. Laszlo, T. Nakajima, and H. Maring (2009). Uncertainties in satellite remote sensing of aerosols and impact on monitoring its long-term trend: a review and perspective, *Ann. Geophys.*, 27, 2755-2770.

Mishchenko, M., and I. V. Geogdzhayev (2007). Satellite remote sensing reveals regional tropospheric aerosol trends. *Optics Express*, 15, No. 12, 7423-7438.

Mishchenko, M., I. V. Geogdzhayev, W. B. Rossow, B. Cairns, B. E. Carlson, A. A. Lacis, L. Liu, L. D. Travis (2007). Long-term satellite record reveals likely recent aerosol trend. *Science*, 315, 1543.

Molling, C.C., Heidinger, A.K., Straka III, W.C. and Wu, X (2010). Calibrations for AVHRR channels 1 and 2: review and path toward consensus. *International Journal of Remote Sensing*, in press.

Pavolonis, Michael J.; Heidinger, Andrew K. and Uttal, Taneil (2005). Daytime global cloud typing from AVHRR and VIIRS: Algorithm description, validation, and comparisons. *Journal of Applied Meteorology*, 44 (6), 804-826.

Pavolonis, Michael J. and Heidinger, Andrew K. (2004). Daytime cloud overlap detection from AVHRR and VIIRS. *Journal of Applied Meteorology*, 43(5), 762-778.

Remer, L. A., D. Tanre, Y. J. Kaufman, C. Ichoku, S. Mattoo, R. Levy, D. A. Chu, B. N. Holben, O. Dubovik, A. Smirnov, J. V. Martins, R-R. Li, Z. Ahmad (2002). Validation of MODIS aerosol retrieval over ocean. *Geophys. Res. Lett.*, 29, doi:10.1029/2001GL013204.

Torres, O., P. K. Bhartia, J. R. Herman, A. Sinyuk, P. Ginoux, and B. Holben (2002). A long-term record of aerosol optical depth from TOMS observations and comparision to AERONET measurements, J. Atmos. Sci., 59, 398-413.

Vermote, E. F., D. Tanre, J. L. Deuze, M. Herman, and J. J. Morcrette (1997a). Second Simulation of the Satellite Signal in the Solar Spectrum, 6S: An overview. *IEEE Trans. Geosci. Remote Sens.*, 35(3), 675-686.

Vermote, E. F. et al. (1997b). *6S User Guide*, Version 2.

Zhao, X., L. L. Stowe, A. B. Smirnov, D. Crosby, J. Sapper, and C. R. McClain (2002). Development of a global validation package for satellite oceanic aerosol optical thickness retrieval based on AERONET observations and its application to NOAA/NESDIS operational aerosol retrievals. *J. Atmos. Sci.*, 59, 294-312.

Zhao, X., O. Dubovik, A. B. Smirnov, B. N. Holben, J. Sapper, C. Pietras, K. J. Voss, and R. Frouin (2004). Regional Evaluation of an AVHRR two-channel aerosol retrieval algorithm. *Journal of Geophys. Res.*, 109, D02204, doi:10.1029/2003JD003817.

Zhao, X., I. Laszlo, P. Minnis, L. Remer (2005a). Comparison and analysis of two aerosol retrievals over the ocean in the Terra/CERES-MODIS Single Scanner Footprint (SSF) data: Part-I – Global evaluation. *Journal of Geophys. Res.*, doi:10.1029/2005JD005851.

Zhao, X., I. Laszlo, P. Minnis, L. Remer (2005b). Comparison and analysis of two aerosol retrievals over the ocean in the Terra/CERES-MODIS Single Scanner Footprint (SSF) data: Part-II – Regional evaluation. *Journal of Geophys. Res.*, Doi:10.1029/2005JD005852.

Zhao, X., I. Laszlo, W. Guo, A. Heidinger, C. Cao, A. Jelenak, D. Tarpley, J. Sullivan (2008). Study of Long-term Trend in Aerosol Optical Thickness Observed from Operational AVHRR Satellite Instrument. *J. Geophys. Res.*, 113, D07201, doi:10.1029/2007JD009061.

Zhao, T. X.-P., A. Heidinger, and K. P. Knapp (2011). Long-term Trends of Zonally Averaged Aerosol Optical Thickness Observed from Operational Satellite AVHRR Instrument. *Meteoro. Appl.*, in press.